

# Distinguishing Coupled Ocean-Atmosphere Interactions from Background Noise in the North Pacific

David W. Pierce

*Climate Research Division, Scripps Institution of Oceanography, La Jolla, California, USA*

---

## Abstract

When considering physical mechanisms for decadal-timescale climate variability in the North Pacific, it is useful to describe in detail the expected response of the ocean to the chaotic atmospheric forcing. The expected response to this white-noise forcing includes strongly enhanced power in the decadal frequency band relative to higher frequencies, pronounced changes in basin-wide climate that resemble regime shifts, preferred patterns of spatial variability, and a depth-dependent profile that includes variability with a standard deviation of 0.2–0.4 C over the top 50–100 m. Weak spectral peaks are also possible, given ocean dynamics. Detecting coupled ocean-atmosphere modes of variability in the real climate system is difficult against the spectral and spatial structure of this “null-hypothesis” of how the ocean and atmosphere interact, especially given the impossibility of experimentally decoupling the ocean from the atmosphere. Turning to coupled ocean-atmosphere models to address this question, a method for identifying coupled modes by using models of increasing physical complexity is illustrated. It is found that a coupled ocean-atmosphere mode accounts for enhanced variability with a time scale of 20 years/cycle in the Kuroshio extension region of the model’s North Pacific. The observed Pacific Decadal Oscillation (PDO) has many similarities to the expected noise-forced response and few similarities to the model’s coupled ocean-atmosphere variability. However, model deficiencies and some analyses of observations by other workers indicate that the possibility that part of the PDO arises from a coupled ocean-atmosphere mode cannot be ruled out.

*Key words:* Climate Variability, Climate Prediction, Climate Change, Pacific, North Pacific

---

## 1 Introduction

In attempting to understand climate variability beyond El Niño, decadal-timescale variability starts to come into play. Decadal variability is ubiquitous in the climate system, and has important implications for society. It includes such features as multi-year droughts and slow changes in oceanic ecosystems that can have profound effects on the local marine populations. In the North Pacific, low-frequency variability is associated with changes in salmon catch over a large area (Mantua, Hare, Zhang, Wallace, & Francis, 1997), with the attendant economic consequences, and with low-frequency variability in wintertime temperature and precipitation over North America (Latif & Barnett, 1994, 1996). A number of groups now produce operational forecasts of El Niño (see, for example, Barnston, Glantz, & He (1999)) and such forecasts can show good predictive skill at lead times of a year or beyond. Can the decadal-timescale variability be predicted as well as this, or does it arise exclusively from the ocean's response to chaotic atmospheric forcing, with no predictability beyond persistence?

To answer these questions, the source of decadal timescale variability must be identified. Variability that ultimately arises from the chaotic forcing of short-term weather variability is unpredictable on decadal timescales, and so must be treated as noise. The manifestations of this noise in the real climate system must be understood in order to avoid attributing complex physical causes to random variations. On the other hand, there is evidence from both coupled ocean-atmosphere general circulation models (O-AGCMs) and observations that there may be coupled modes of interaction between the ocean and atmosphere that produce variability on the decadal timescales. This kind of variability is potentially predictable by coupled O-AGCMs.

The first purpose of this paper is to illustrate in a specific way the effects that noise forcing can have on the physical (and hence biological) environment of the North Pacific. The North Pacific is chosen because significant variations on this timescale have been well documented (e.g., Ebbesmeyer, Cayan, McLain, Nichols, Peterson, & Redmond, 1991; Trenberth & Hurrell, 1994; Miller, Cayan, Barnett, Graham, & Oberhuber, 1994). The second purpose is to demonstrate a methodology by which it can be determined if a particular aspect of variability arises from internal atmospheric noise, atmospheric noise impinging on a passive ocean, atmospheric noise impinging on a dynamic ocean, or fully coupled ocean-atmosphere interactions. Illustrations of each kind of variability will be given. A key point will be that it is difficult to find conclusive evidence for coupled ocean-atmosphere modes given the strong noise background.

Note that in other regions different physical processes might cause climactic

variability on decadal timescales; for example, variations in the thermohaline circulation in the North Atlantic (Delworth, Manabe, & Stouffer, 1997), or the Antarctic circumpolar wave in the southern hemisphere (White & Peterson, 1996). In the tropical regions, decadal variability in ENSO is known to occur (e.g., Zhang, Wallace, & Battisti, 1997; Goddard & Graham, 1997), which will have an influence on the North Pacific via atmospheric teleconnections. Additionally, there may be low-frequency climatic variability arising from mechanisms extrinsic to the coupled ocean-land-atmosphere system; for example, solar variability (Cubasch, Voss, Hegerl, Waszkewitz, & Crowley, 1997), or irregular volcanic activity, which can have major impacts on the climate. These mechanisms will not be examined here given the specific purposes of this paper described above. A review of these and other dynamical mechanisms for producing low-frequency climate variability in the North Pacific is given in Miller & Schneider (2000). Previous studies that have addressed the predictability issue include Venzke, Munnich, & Latif (1999), who examine the change in climate of the North Pacific in the late 1970s, and Grotzner, Latif, & Timmermann (1999), who use coupled models to estimate levels of predictability over the world's oceans.

This paper is laid out as follows. In Section 2 noise-forced variability is described, including the spectrally white atmospheric forcing, the red-noise response in the ocean, and two “stochastic-dynamic” theories that predict a spectral peak given white atmospheric forcing and ocean dynamics. In Section 3 the issue of attributing variability to these various mechanisms is addressed using a hierarchy of ocean-atmosphere models of increasing complexity. The results are discussed in Section 4, including an evaluation of the Pacific Decadal Oscillation in terms of the expected noise-forced variability. Conclusions are given in Section 5.

## 2 Noise Forced Variability

### 2.1 *White-Noise Atmospheric Forcing*

At forecast lead times greater than a few weeks, the detailed evolution of the atmosphere is unpredictable. (In this and the following sections, quantities will be taken as departures from the climatological mean for the appropriate time of year, so the strong effect of the annual cycle is removed.) Therefore, on time scales  $>1$  month, weather variability can be considered a random forcing of the climate system that can only be described statistically, for example in terms of the autocorrelation timescale and the distribution of power as a function of frequency (the spectrum).

Over much of the Pacific, many atmospheric variables have equal power at all frequencies (within the expected sampling errors given the finite record length), which is to say, they have white spectra. It is sometimes said that the atmosphere by itself cannot be the source of decadal timescale climate variability because it “has no memory” on such timescales. This is untrue; the intrinsic variability of the atmosphere results in decadal variability, since a white spectrum has as much power in the decadal frequency band as in every other band. The relevant question is whether there is more variability in the decadal frequency band than is expected; this can only be answered after the expectation is made clear. As shown in the following two sections, the interaction of white noise atmospheric forcing with the ocean is expected to strongly emphasize decadal timescale variability.

## 2.2 Red-Noise Oceanic Response

Hasselmann (1976) and Frankignoul & Hasselmann (1977) laid the foundations for calculating the response of the midlatitude oceans to a white-noise atmospheric forcing. The basic idea is straightforward. Imagine a bucket of water exposed to the atmosphere. Considering for the moment only heat fluxes through the surface, and assuming that some unspecified mechanism keeps the bucket well mixed, the change in water temperature anomaly  $T_o$  can be related to the surface heat flux  $Q$  as follows:

$$\frac{dT_o}{dt} = \frac{Q}{\rho_o c_p \Delta z} - \lambda T_o, \quad (1)$$

where  $\rho_o$  is the density and  $c_p$  the specific heat of water,  $\Delta z$  is the depth of the water in the bucket, and  $\lambda$  represents a damping time to climatological conditions (at which the temperature anomaly  $T_o = 0$ .) The damping can be thought of as sensible and latent heat loss to the atmosphere if the bucket is small enough (in the latitude-longitude extent) to have little effect on the overlying atmosphere, or as longwave radiative loss to space if the bucket is large enough (say, a radius of 1000 km or more) for water temperatures to appreciably influence the overlying atmosphere (Pierce, Kim, & Barnett 1996).

Now assume that the surface heat flux forcing  $Q$  is white noise:  $\hat{Q}(\omega) = \epsilon$ , where  $\hat{Q}$  is the Fourier transform of  $Q$ ,  $\omega$  is the frequency, and  $\epsilon$  is a constant describing the overall power in  $Q$ . To find the spectrum of  $T_o$ , simply Fourier transform Eq. 1 to obtain:

$$P = \frac{\epsilon}{\rho_o c_p \Delta z \sqrt{\lambda^2 + \omega^2}}, \quad (2)$$

where  $P$  is the power in  $T_o$  (i.e., the magnitude of  $\hat{T}_o$ ). For very low frequencies ( $\omega \ll \lambda$ ),  $P \rightarrow \epsilon/(\rho_o c_p \Delta z \lambda)$ , which is a constant. For high frequencies ( $\omega \gg \lambda$ ),  $P \sim 1/\omega$ . This is plotted in Fig. 1, and will hereafter be termed a red-noise spectrum. Physically, having a white-noise forcing but red-noise response does not mean that high frequency energy is being transferred to low frequencies in order to enhance the power there. Rather, forcing at frequencies higher than the natural timescale of the system are preferentially damped, while those lower than the natural timescale are not. This results in a reshaping of a white forcing spectrum into a red response spectrum.

In the context of decadal climate variability, the red-noise response of the ocean to spectrally white atmospheric forcing is particularly troublesome because the “knee” of the spectrum shown in Fig. 1 — the frequency at which the power as a function of frequency changes from  $1/\omega$  to a constant — typically falls close to the decadal range. Also, the number of oceanic observations in most regions drops sharply for times more than 40-50 years ago. The result is spectra that tend to reach maximum values in the decadal time band, then run out of data at lower frequencies, leading to the impression of a decadal peak in the spectrum. For example, consider the spectrum expected for ocean temperatures in the North Pacific as modeled by Eq. 1. For basin-scale perturbations, the coupling between the ocean and atmosphere is about  $\kappa = 2.6 \text{ W m}^{-2} \text{ C}^{-1}$  (Pierce et al. 1996); the seasonal cycle of temperature is visible down to  $O(150 \text{ m})$ , so this is a reasonable lower bound to take for  $\Delta z$ , leading to  $\lambda = \kappa/(\rho_o c_p \Delta z) \approx 8 \text{ yr}^{-1}$ .

An illustration of this basic red-noise character of many observed data sets in the North Pacific is given in Fig. 2, which is the spectrum of the “Pacific Decadal Oscillation” (PDO; Mantua et al. (1997)) sea surface temperature (SST) based time series over the years 1900-1997.<sup>1</sup> The heavy line is the best-fit red noise spectrum based on a first order autoregressive process (AR(1)); the dashed lines indicate the 95% confidence intervals based on sampling uncertainty given the finite record length. The only statistically significant departure from a red noise spectrum occurs at a period of about 7 years/cycle; no lower-frequency (or decadal, in particular) signature can be positively identified by this technique. (The issue of whether the PDO has components beyond this red-noise background is discussed in Section 4.)

The subjective character of red-noise time series of this type is that they appear to undergo “regime shifts” that seem to require detailed physical mechanisms, but are actually just noise. This is illustrated in Fig. 3, which shows five century-long time series, one of which is the actual PDO time series, and the other four of which were generated with a random number generator set to have the same AR(1) characteristics as the PDO (the lag one autocorrela-

---

<sup>1</sup> Data obtained from [ftp://ftp.atmos.washington.edu/mantua/pnw\\_impacts/INDICES/PDO.latest](ftp://ftp.atmos.washington.edu/mantua/pnw_impacts/INDICES/PDO.latest).

tion coefficient is 0.50). The heavy line is the seven year boxcar average of the individual years.

Examination of these series shows that it is difficult to pick out the true PDO time series by eye, as the random time series appear to have the same kind of low-frequency behavior and sudden “regime shifts” as the PDO. For example, for time series B, there is apparently a strong “regime shift” going from low values in the 1950s to high values after year 1960, and the record in general has a pronounced oscillatory nature with a period of  $\sim 20$  years/cycle. For time series C, there is a strong regime shift going from low values in the 1940s to high values 1955-1965. For time series D, the eye tends to pick out a trend, with the highest values in the 1920s decreasing to the lowest values in the 1990s; one might imagine that if this series were to be obtained on a planet with observed global warming, there would be a temptation to identify this trend as a consequence of global warming. For time series E, there is a very pronounced regime shift in 1930, with almost uniformly high values giving way abruptly to a decade of low values.

Spectra of the time series of Fig. 3 are shown in Fig. 4, calculated using the multi-taper spectral method (Ghil, 1997). It can be seen that time series A is identified as having one peak significant at the 95% level; series B as having 3; series C as having 2; series D as having 3; and series E as having 4. In point of fact, the true PDO time series is C, which has been plotted backwards in Fig. 3 so that immediate identification of the series by readers familiar with it would be avoided (for example, the famous shift in North Pacific conditions in the late 1970s can be seen happening in the early 1920s). Synthetic series B, D, and E all were identified as having more spectral peaks significant at the 95% level than the true PDO; and from Fig. 3, several of the pure noise time series seem to have “regime shifts” as significant and convincing as the true PDO.

This exercise with randomly generated time series serves to illustrate that the *expected* red-noise characteristics of many North Pacific oceanic variables can give rise to apparent “regime shifts.” Clearly there is no deterministic physical meaning attached to the shifts obtained from the random series; by inference, the attempt to assign deterministic physical meaning to the shift observed in the North Pacific during the late 1970s should be approached with caution unless the shift can be shown to have characteristics unlike red noise.

One final caveat is worth mentioning. The atmosphere, ocean, and ecology of the North Pacific are a coupled physical system. Therefore, any diagnosis of internal events in this system will necessarily find a causal chain of physical actions and reactions. The relevant question for our purposes is whether all these actions can be ultimately traced back exclusively to unpredictable atmospheric variability, rather than predictable atmospheric variability (asso-

ciated with ENSO or another coupled ocean-atmosphere mode, for example) or oceanic processes.

Miller et al. (1994) and Deser, Alexander, & Timlin (1996) do such analyses of the ocean-atmosphere system, and find results consistent with the idea that most of the change observed in the North Pacific ocean in the late 1970s was ultimately forced by the atmosphere, with regional modifications due to the dynamic oceanic response to the forcing. Mantua et al. (1997) does an analysis using the ecological response as the “effect” and changes in the North Pacific’s ocean environment as the “cause,” and found results that are consistent with the idea that changes in the physical environment forced the ecological response. Taken in conjunction with the Miller et al. and Deser et al. results, this supports the idea that the decadal timescale ecological changes that Mantua et al. analyzed are ultimately due to the variable atmospheric forcing, with a relatively small contribution from ocean dynamics. Keeping in mind the red-noise characteristics *expected* of these processes (Fig. 3), a large fraction of this variability is likely explainable as noise, and has no deeper physical interpretation than that. However, some part of the variability examined by Mantua et al. might still arise from processes that depend on interaction between the ocean and atmosphere; this question will be addressed in Section 4.

### 2.3 Stochastic Resonance Theories

The previous section was concerned with the case of atmospheric forcing of an ocean with no dynamics, only thermodynamics. The result is a red-noise spectrum in oceanic variables such as SST. When ocean dynamics are added to the system, work by Saravanan & McWilliams (1998) and Weng & Neelin (1998) demonstrate that a spectral peak can be generated even in the absence of feedbacks from the ocean to the atmosphere. This complicates the detection of (potentially predictable) coupled ocean-atmosphere modes, because it means that the existence of such a spectral peak is not by itself enough to infer the existence of a coupled mode.

The basic idea behind the stochastic resonance theories is straightforward. For a spectral peak to be generated – i.e., for a preferred timescale to be selected by the system – there are two requirements. First is that the atmospheric forcing have a preferred large-scale spatial pattern (despite the fact that, temporally, there is no preferred time scale to the forcing). Second is that there be some oceanic mechanism that moves information underneath the atmospheric pattern. For Saravanan et al. (1998), the oceanic mechanism is advection by the mean gyre; for Weng et al. (1998), the mechanism is Rossby wave propagation.

The first requirement, of a large-scale spatial pattern to the forcing, is generally

met in the world’s oceans. Fig. 5, for example, shows the leading empirical orthogonal function (EOF) of latent heat flux from the ECHO2 coupled ocean-atmosphere model (Frey, Latif, & Stockdale 1997; Pierce, Barnett, & Latif 2000a). There is a distinct pattern with opposite signs in the eastern and western parts of the basin. Weng et al. (1998) show other examples in the North Atlantic.

The way in which the large-scale forcing pattern and the movement of information combine to produce a preferred timescale is easily understood. Consider a simplified example with information moving from west to east along the heavy line in Fig. 5. If the water parcel or Rossby wave experiences the *same sign* of forcing all along its path, the response to the forcing will be greater than if there is some forcing of one sign and some forcing of the other sign, which will have a tendency to cancel.

The speed of the parcels or wave is set by the gyre advection time, Rossby wave dynamics, or some other oceanic process, and is approximately a fixed number independent of the surface forcing. Therefore, to experience only one sign of forcing during transit (and thus have the maximum response), the forcing must *change sign* when the parcel or wave has traveled from the eastern boundary to the zero-crossing point of the forcing (about 170W in Fig. 5). If the time it takes to travel from the eastern to western boundary is  $t$ , we can approximate the time it takes to get to the zero-crossing point as  $t/2$ . In that case, the the maximum response will be obtained when the forcing has a frequency such that one-half cycle takes  $t/2$ , i.e., a frequency of  $1/t$ . Keep in mind that the actual forcing has all frequencies at equal power; the point is that the particular *component* of the forcing that has a frequency of  $t^{-1}$  is preferentially amplified by this mechanism, resulting in a spectral peak at that frequency. For the mechanisms considered by Saravanan et al. (1998) and Weng et al. (1998), these frequencies typically fall in the decadal range.

#### 2.4 *Summary of Noise-Forced Oceanic Response*

The response of the ocean to noisy atmospheric forcing is expected to include enhanced power at decadal frequencies, behavior that appears similar to “regime shifts,” preferred spatial patterns imposed by the preferred patterns of internal atmospheric variability, and even decadal-timescale spectral peaks. Although a causal chain of physics can be internally diagnosed for this low-frequency variability, in the larger picture it is nothing more than unpredictable noise. From the forecasting point of view, the only gain is from the enhanced persistence of the ocean’s integrated response to the forcing. This is problematic if one wants to identify (potentially predictable) coupled ocean-atmosphere modes of variability, as such modes might be thought to be



identifiable by spectral peaks or preferred spatial patterns of variability. The next section will present a methodology that can be used to identify coupled ocean-atmosphere modes in the presence of the strong red-noise background.

### 3 Attributing Causes of Decadal Climate Variability

Given the difficulty of separating a coupled ocean-atmosphere mode of variability from the background noise, how can any such coupled mode be identified? An approach will be demonstrated here that makes use of a hierarchy of coupled models with an increasing degree of ocean physics. The simplest level is a full-physics atmospheric model coupled to specified climatological SST conditions as a lower boundary condition. Any variability that develops in this scenario will be due to internal atmospheric dynamics alone. The intermediate level of model is the same atmospheric model coupled to a mixed-layer ocean model, preferably one with a realistic mixed-layer depth that varies by season. Any variability that appears in this run that did not appear in the specified-SST boundary condition run must arise from the effects of ocean thermodynamics. Models of this complexity will evolve the red-noise spectra described by Hasselmann (1976) and Frankignoul et al. (1977). The most complex level is to couple the atmosphere to a full physics oceanic general circulation model. New patterns or levels of variability that appear in this case are arising from mechanisms above and beyond the expected red-noise background, and (since ocean dynamics is present) may come from stochastic resonance as described by Saravanan et al. (1998) and Weng et al. (1998), from fully coupled ocean-atmosphere modes, or from dynamic internal ocean variability (if the model resolution is high enough to permit it).

Previous related work has often focused on the influence of various geographical regions on low-frequency variability, using either climatological or specified observed SSTs or mixed-layer ocean models in the different regions. For example, Graham, Barnett, Wilde, Ponater, & Schubert (1994) and Lau (1997) examined the influence of specifying tropical versus extratropical (and especially North Pacific) SST anomalies, while Blade (1997) examined the influence of midlatitude ocean thermodynamics on low-frequency variability in a coupled model. Grotzner et al. (1999) was interested in predictability rather than the relative influence of various geographical regions, and so compared his fully-coupled model results to those expected from first-order autoregressive (red-noise) processes. The objective here is somewhat different in that an identification of the source of low-frequency variability is desired, and thus an intercomparison of results with specified SST, mixed layer, and full ocean physics is needed. This is more akin to the work of Barnett, Pierce, Saravanan, Schneider, Dommenges, & Latif (1999), who also did some forced-atmosphere tests of a coupled ocean-atmosphere mode they identified.

### 3.1 *Internal Atmospheric Variability*

When an atmospheric model has prescribed monthly climatological SSTs as a lower boundary condition, the only mechanism that allows variability is internal atmospheric dynamics. This is the case in the top left panel of Fig. 6, using a 199 year run of CCM3 (Kiehl, Hack Bonan Boville Briegleb Williamson Rasch et al., 1996). Plotted is the leading EOF of 500 mb height anomaly (in gpm), normalized so that the associated principal component (PC) has a standard deviation of 1. The pattern is similar to the PNA (Horel & Wallace, 1981), and in this case is known to arise exclusively from atmospheric variability because no other processes are included in the model.

### 3.2 *Ocean Response to Atmospheric Variability*

When a mixed layer ocean (with mixed layer depths specified from monthly climatology (Levitus, 1994)) is joined to the same atmospheric model, the pattern of variability is unmodified (Fig. 6, middle left panel), leading to the conclusion that even in the presence of ocean thermodynamics, the pattern is set by internal atmospheric variability. The strength of the variability increases by about 25%. This can be understood from the arguments of Barsugli & Battisti (1998); a lower boundary condition that is free to change temperature in response to surface fluxes provides less damping than a fixed-SST condition. The SST pattern associated with this atmospheric variability is shown in the middle right panel of Fig. 6, obtained by correlating the EOF's PC with SST at all points. Since there are no ocean dynamics in this case and the pattern of forcing is set by the atmosphere, the SST response is best described as the ocean's passive thermodynamic response to internal atmospheric variability. This response is similar to the North Pacific mode (Deser & Blackmon, 1995), as identified in this model run by Pierce, Barnett, Schneider, Saravanan, Dommenget, & Latif (2000b).

When full ocean physics are added (Fig. 6, bottom left panel) the pattern of atmospheric variability is again unmodified but strengthened by about 20%. Since the coupled ocean-atmosphere model allows ENSO variability, part of this increase in strength comes from teleconnected tropical variability exciting this same atmospheric response. The associated SST pattern is shown in the bottom right panel of Fig. 6, and looks similar to the case without ocean dynamics. In the southern hemisphere (not shown) there is a hint of more organized symmetry about the equator, which is consistent with the idea that part of the signal now is associated with tropical forcing, but none of the values south of 20 N is statistically significant.

The three-dimensional structure of the oceanic temperature response to atmospheric variability can be of interest when evaluating the possible biological effects. How deep does the oceanic response go, and how large are the temperature excursions at depth? This can be found by correlating the PC of the model's leading 500 mb height anomaly EOF with oceanic temperatures as a function of depth, which are available when the full physics ocean model is used. Values between 0.45 and 0.60 are found over the top 50 to 100 m, depending on location. These values are significant at the 95% level, taking the degrees of freedom to be 18 based on the PC's autocorrelation function and the model run length. The correlations drop off rapidly at deeper levels. These simultaneous correlations do not take into account any lag that might be expected for the vertical propagation of information in the ocean. Note also that in this case, since full ocean dynamics are present, some of this response is coming from teleconnected ENSO activity in the tropics. Since the teleconnection would be expected to act through the atmosphere, the estimate given above that the strength of the atmospheric response increases by about 20% when ocean dynamics are present gives a reasonable estimate for the strength of the oceanic response coming from the teleconnected effect versus local internal atmospheric variability.

In the real ocean, the teleconnected ENSO effect is likely stronger than in the coupled model, and other physics not well represented in the model may come into play. Thus, identification of the effects of internal atmospheric variability cannot be made with certainty, as some of this other physics might have a response that projects onto the patterns generated by internal atmospheric variability. Keeping these important caveats in mind, an attempt can nonetheless be made to look at these same relationships from the observed record. Used here are sea level pressure (SLP) anomalies from da Silva, Young, & Levitus (1995) and the upper-ocean temperature data set of White (1995). This three-dimensional data set of ocean temperatures is used because it is again of interest to see how deep the signal penetrates. For SST only, previous work by others (e.g., Wallace, Smith, & Jiang (1990)) using observations has already identified relationships between 500 mb height anomaly and SST that are similar to Fig. 6.

The regression between the PC of the leading EOF of observed SLP and ocean temperatures as a function of depth along 40 N is shown in Fig. 7. Values are given in degrees C for one standard deviation of the principal component of the leading EOF of sea level pressure. The values range from 0.2 to 0.4 C per standard deviation, and penetrate 50-100 m, similar to the model results. There is some tendency for peak values to occur subsurface, as can be seen in the plot at about 130 W. This may arise from stronger variability of the forcing atmospheric pattern in winter, when the mixed layer is deeper.

In summary, the patterns of atmospheric and oceanic variability shown in

Fig. 6 are set by internal atmospheric variability, to which the ocean responds via surface heat fluxes. This is the red-noise oceanic response described by Hasselmann (1976) and Frankignoul et al. (1977). Because the atmosphere has a preferred spatial pattern of variability, the oceanic response does as well, despite the fact that ocean dynamics are not necessary for this pattern's genesis. The addition of ocean dynamics increases the strength of the pattern by about 20% in the model, some of which is due to teleconnected forcing from the tropics. The vertical structure of the ocean's response encompasses the top 50 to 100 m, and has a standard deviation in the range 0.2-0.4 C.

### 3.3 Variability due to Ocean Dynamics

The addition of ocean dynamics to the ocean-atmosphere system allows for new kinds of variability, which may be coupled ocean-atmosphere modes or the kind of stochastic resonance phenomena described by Saravanan et al. (1998) and Weng et al. (1998). The geographical distribution of this enhancement can be found by dividing the standard deviation of SST anomalies for the model with full atmosphere-ocean dynamics by the same quantity for the atmosphere coupled to a mixed layer ocean. Values greater than one signify regions where variability is enhanced when ocean dynamics is added.

This ratio is illustrated in Fig. 8. The run with full ocean-atmosphere physics is ECHO2 (Frey et al. 1997; Pierce et al. 2000a), which uses the ECHAM4 atmospheric model coupled to the HOPE ocean model. The mixed-layer run uses ECHAM3 coupled to a mixed layer ocean model with a fixed 50 m depth (this run is described further in Pierce et al. 2000b). Because of the different versions of atmospheric models used and the fixed mixed layer depth, this is not an ideal comparison. In particular, wintertime mixed layer depths in the North Pacific can easily be three times the fixed 50 m depth assumed in the mixed layer model; this will tend to exaggerate variability in the mixed layer run, which reduces the ratio in Fig. 8. Nevertheless, these runs are used here for exact comparison with the time-permuted run using the HOPE ocean model (described below). (For the CCM3-based runs, the ratio of standard deviations is a more direct comparison, and shows the same enhanced variability off Japan but lacks the enhancement in the central Pacific. It also shows enhanced variability in the Gulf of Alaska that is likely a model error, as erroneous model sea-ice formation known to occur in this region.)

Fig. 8 shows that there are regions of enhanced variability due to ocean dynamics in the sub arctic frontal zone (SAFZ)/Kuroshio extension region off Japan and in the central Pacific. The enhanced variability in the central Pacific has spectral peaks in the 2-7 years/cycle band, and is in the location expected to show teleconnected effects of ENSO variability (Blackmon, Geisler, & Pitcher,

1983), and so will be presumed to be due to this cause.

The variability off Japan is of some interest, as previous work has shown that the atmosphere may be sensitive to SST anomalies in this region at certain times of the year (Peng, Robinson, & Hoerling, 1997). Such atmospheric sensitivity to oceanic SST anomalies is required in order to have a coupled ocean-atmosphere mode. The frequency at which this enhancement is occurring can be obtained by dividing the spectral density as a function of frequency in the case with full ocean physics to the same quantity in the mixed layer case. This is shown in Fig. 9, plotted at the point 156 W, 40.5 N (in the heart of the enhancement region off Japan shown in Fig. 8). Statistical significance is assessed by noting where the 90% confidence intervals for the two spectra do *not* overlap. The variability is preferentially enhanced at a frequency of  $\sim 20$  years/cycle. The difference in frequency between this spectral peak and the ENSO spectral peaks (3-7 years/cycle) suggests that this is not a direct ENSO-forced response.

This result is in general accord with that found in Latif et al. (1994, 1996), who proposed a basin-wide ocean-atmosphere coupled mode in the North Pacific that produces a time scale of about 20 years/cycle. Enhanced spectral power at this frequency only in the presence of ocean dynamics, such as is documented here, would be one of the hallmarks of such a coupled mode. On the other hand, the spectral enhancement seen here is confined to the most western part of the basin, which is not simply consistent with a basin-wide mode. This could be a detection issue – i.e., the signal could be generally present over the entire North Pacific, but more easily detectible in the western boundary region. This might be because strong SST gradients in the region make small circulation perturbations more easily visible, or because of the tendency for Rossby waves to carry information preferentially to the west. Or, instead of being a detection issue, the western trapping of the signal seen here might indicate that the signal is due to some other process than found in (Latif et al., 1996), such as stochastic resonance. This question will now be addressed.

Having identified a pattern of oceanic variability that has a preferred decadal frequency and arises only in the presence of ocean dynamics (i.e., variability that is *not* the red-noise response of Hasselmann (1976) and Frankignoul et al. (1977)), it remains to be determined whether it is caused by stochastic resonance mechanisms or by some kind of coupled ocean-atmosphere interaction. In this, use can be made of the property that stochastic resonance mechanisms depend only on the existence of preferred spatial patterns in the atmospheric forcing fields and arise even if the forcing fields have equal power at all frequencies. If (and only if) it can be confirmed that the atmospheric forcing fields actually do have white spectra, then it is legitimate for the purposes of this test to randomly permute the forcing fields in time, since this changes neither the spatial nor spectral structure of the forcing. Under these conditions

the stochastic resonance mechanism would proceed unchanged, assuming that the time chunks to be permuted are long compared to synoptic atmospheric variability but still short compared to frequencies in the signal of interest. If the forcing fields are permuted in time and the oceanic SST response still has the same spectral peak, it can be concluded that the peak arises from a stochastic resonance mechanism. If the spectral peak disappears, the peak must arise from some process that requires synchronous evolution of the ocean and atmosphere, i.e., a coupled ocean-atmosphere mode of variability.

The frequency of interest here is  $\sim 20$  years/cycle, so the surface forcing anomaly fields (wind stress, heat flux, and P-E) were permuted in monthly-average chunks. In the ECHO2 run, spectral analysis of the surface forcing flux anomaly fields show that they have white spectra over almost all of the North Pacific, thus meeting the requirement for the time-permuted test. The exception to this is in the Kuroshio extension region itself, where it is found that the heat fluxes have the same  $\sim 20$  year/cycle spectral peak as found in the SSTs. The phasing of the two is such that in this region, warm SST anomalies cool by surface heat loss to the atmosphere. Therefore, the process causing the spectral peak in the surface heat fluxes plays no part in *generating* the SST anomalies in the first place; it only serves to damp the anomalies. In fact, in this region the time-permutation procedure will cause SST anomalies to be less systematically damped, possibly acting to increase the magnitude of any spectral peak that might be generated by stochastic resonance. Therefore, removing this signal by time-permutation will not weaken any mechanism that is forcing the SST variability in the first place, and the lack of a spectral peak in the results will still indicate the presence of a coupled ocean-atmosphere mode.

The results of forcing the HOPE model with randomly permuted surface flux forcing fields saved from the ECHO2 run are shown in Fig. 10. The top panel shows the spectrum of the SST anomalies in the ECHO2 model in the Kuroshio extension region (142E to 164E, 32N to 46N), for comparison. The spectral peak at  $\sim 20$  years/cycle can be seen. The center panel shows the results from a control experiment imposing the saved monthly fluxes in temporal order. The same peak is seen, demonstrating that the technique of forcing the model with monthly saved fluxes can reproduce the signal of interest. The bottom panel shows the results of the experiment with time-permuted surface fluxes. The spectral peak is no longer present. The conclusion to be drawn from this is that the spectral peak arises from some mechanism that requires time synchronicity between the ocean and the atmospheric forcing fields, i.e., a coupled ocean-atmosphere mode.

In summary, ocean dynamics adds preferred regions and timescales of variability onto the red-noise background signal generated by internal atmospheric variability. In the model context, the possibility that this timescale arises from stochastic resonance mechanisms can be tested by permuting the surface flux

forcing fields in time, if and only if the forcing fields are spectrally white. This is the case in the ECHO2 run, and it is found that the spectral peak arises from a coupled ocean-atmosphere interaction. Further analysis could then be used to see if the interaction is consistent with that described by various theories, such as Latif & Barnett (1994, 1996), Jin (1997), or Goodman & Marshall (1999).

## 4 Discussion

The treatment in Section 2b focussed on the red-noise characteristics of the PDO. However, while the arguments presented there suggest that much of the variance of the PDO may simply be the expected red-noise response to the chaotic atmospheric forcing, that does not answer the question of whether any part of that signal is deterministic, above and beyond the response expected from the noise forcing. The model technique outlined in Section 3b suggested an approach to answer this question, but only for variability seen in a model; since the model's decadal timescale dynamic response is generally confined to the SAFZ/Kuroshio extension region, while the main PDO signal is in the central and eastern Pacific, there is no reason to identify this model response as the "PDO."

This difference between the model's dynamic response and the PDO may be thought to arise from a number of causes. 1) The models may be correct, and the PDO is exclusively noise-forced, while a dynamic response should be seen only in the SAFZ/Kuroshio extension region. 2) The models may err in trapping the dynamic variability too far to the west, perhaps because of poor resolution. The details of horizontal advection by the Kuroshio are lost in models with T42 (approximately  $2.8^\circ$  by  $2.8^\circ$ ) resolution, and may be important to transmitting a signal across the Pacific. The PDO's response along the west coast of North America might involve coastal processes, which are poorly represented at these resolutions. 3) The models may be poorly representing some other, as yet unknown, physics that makes up a coupled ocean-atmosphere mode in the midlatitudes.

Deciding between these possibilities can only be done by model studies at higher resolution and by analyzing the observed record. There is, in fact, some evidence from observations that there may be a part of the PDO that has a distinct decadal time scale and therefore, by inference, arises from a coupled ocean/atmosphere mode of interaction (the arguments of Section 2.3 notwithstanding). Venzke et al. (1999) analyzed wintertime sea level pressures over the North Pacific and found, via singular spectrum analysis, an oscillation with a well-defined 18 year/cycle period. This was the leading mode, and explained 15% of the variance. Considering that the amount of variance explained is

somewhat modest, caution is warranted before immediately concluding that this oscillation can be positively identified as the PDO.

Biondi, Gershunov, & Cayan (2000) analyzed tree ring data from Baja, Mexico — a region whose wintertime temperature and precipitation are known to be strongly correlated with the state of the North Pacific (Latif et al., 1996) — and found a clear spectral peak at about 23 years/cycle. Again, considering the difference in frequency compared to the results from Venzke et al. (1999), caution is indicated before assuming that this signal must reflect the PDO. Biondi et al.’s data is particularly interesting in that his evolutive spectrum over the period 1710-1940 shows a clear and distinct spectral peak *until* 1910, at which time the power in the very lowest frequencies increases to the point where the 23 year/cycle peak is no longer distinctly separated and the spectrum appears red. It is interesting to speculate that this increase in low-frequency power after 1910 may be a manifestation of the observed trend in global temperatures during the 20th century. The linear trend of yearly SST anomalies over the period 1945–1999 (from da Silva et al. (1995) data combined with NCEP data after 1993), shown in Fig. 11, has a strong projection onto the PDO signal; there is cooling in the central Pacific and warming along the west coast of North America. The magnitude of the trend — about 0.3 C over the 23 year timescale Biondi et al. found — is large enough to be important, as the standard deviation of temperatures from the PDO is about 0.4 C. A final resolution this matter will have to await more data of this kind.

## 5 Conclusions

The first objective of this work was to illustrate in a concrete way the characteristics expected of noise-forced oceanic variability in the North Pacific. The expected pattern of ocean response is set by internal atmospheric variability, and consists of a lobe of temperature of one sign extending from Japan into the central Pacific east of the dateline, surrounded on the east by a horseshoe-shaped region of opposite sign. The addition of ocean thermodynamics, and then ocean dynamics, each increase the strength of this pattern by about 20-25% but do not appreciably alter its shape. In the vertical, this signal can be seen in the upper 50–100 m of the water column, depending on location. Typical temperature excursions are in the range of 0.2–0.4 C (for one standard deviation). There is some tendency for the signal to reach a maximum below the surface, perhaps because the mixed layer is deeper in winter, when the surface forcing tends to be stronger. The temporal character of this noise-forced response can exhibit quasi-periodic behavior and pronounced decadal “regime shifts” that have no particular physical significance. Even so, these changes in the physical environment can have a deterministic impact on the local ecology due to associated changes in temperature, turbidity, vertical mixing, advective



transport, stratification, and so on.

The second objective of this work was to demonstrate a methodology for determining if a particular signal arises from intrinsic atmospheric variability, the added effect of ocean thermodynamics, or full ocean dynamics. This was illustrated using model runs with a full-physics atmospheric GCM coupled to ocean models of increasing complexity. Internal atmospheric variability and ocean thermodynamics give rise to the red-noise response described above. However, it was found that some model variability can be attributed to ocean dynamics, including ENSO-related variability (not examined here) and decadal-timescale variability that occurs in preferred locations (the SAFZ/Kuroshio extension region) and with a preferred time scale of about 20 years/cycle. The spectral characteristics of the forcing found in the model allowed a test of the possibility that the preferred timescale arises from a stochastic resonance mechanism. The test made use of the saved monthly surface flux forcing fields permuted in time. The results of this test suggest that the variability arises from an coupled mode of the ocean-atmosphere system.

Finally, the relationship of the observed PDO to these results was considered. The PDO has many characteristics in common with the expected noise-forced response, and so it is likely that much of the variance in the PDO is explainable simply as noise. However, there are some observations that suggest part of the PDO's variability may come from a coupled ocean-atmosphere mode that the models do not correctly simulate. Of particular interest is data from tree rings that suggest the global temperature trend in the 20th century may have masked a distinct spectral peak associated with the PDO, making it merge into an apparent red-noise spectrum. More data sets of this type, and model runs with the resolution required to capture advective and coastal processes in the North Pacific, will be required to settle this issue.

## 6 Acknowledgments

This work benefited from discussions with Tim Barnett, Niklas Schneider, and Arthur Miller of Scripps, which are gratefully acknowledged. This work was supported by the Department of Energy's CCPP Program (DE-FG03-91-ER61215), NSF Grant OCE97-11265, the Scripps Institution of Oceanography, and the German government under its Decadal Predictability grant. The simulations described here were executed at NCAR's Scientific Computing Division (SCD) and Climate Simulation Laboratory (CSL), supplemented with runs at the National Energy Research Scientific Computing Center (NERSC). Thanks are due to Lennart Bengtsson and Erich Roeckner for supplying the ECHAM4 atmospheric model.

Barnett, T.P., Pierce, D.W., Saravanan, R., Schneider, N., Dommenges, D., & Latif, M. (1999). Origins of the midlatitude Pacific decadal variability. *Geophysical Review Letters*, 26, 1453–1456

Barnston, A.G., Glantz, M.H., & He, Y. (1999). Predictive skill of statistical and dynamical climate models in SST forecasts during the 1997-98 El Nino episode and the 1998 La Nina onset. *Bulletin of the American Meteorological Society*, 80, 217–243

Barsugli, J., & Battisti, D.S. (1998). The Basic Effects of Atmosphere-Ocean Thermal Coupling on Midlatitude Variability. *Journal of the Atmospheric Sciences*, 55, 477–493

Biondi, F., Gershunov, A., & Cayan, D.R. (2000). Winter PDO reconstructed from southern california tree-ring records. *Progress in Oceanography*

Blackmon, M.L., Geisler, J.E., & Pitcher, E.J. (1983). A general circulation model study of January climate anomaly patterns associated with interannual variation of equatorial Pacific sea surface temperatures. *Journal of the Atmospheric Sciences*, 40, 1410–1425

Blade, I. (1997). The influence of midlatitude ocean-atmosphere coupling on the low-frequency variability of a GCM. Part I: No Tropical SST forcing. *Journal of Climate*, 10, 2087–2106

Cubasch, U., Voss, R., Hegerl, G.C., Waszkewitz, J., & Crowley, T.J. (1997). Simulation of the influence of solar radiation variations on the global climate with an ocean-atmosphere general circulation model. *Climate Dynamics*, 13, 757–767

da Silva, A.M., Young, C.C., & Levitus, S. (1995). Atlas of Surface Marine Data 1994, Volume 1: Algorithms and Procedures.. Technical Report ””, Available from NOAA Atlas NESDIS 6, U.S. Dept. Commerce.

Delworth, T.L., Manabe, S., & Stouffer, R.J. (1997). Multidecadal climate variability in the Greenland Sea and surrounding regions: a coupled model simulation. *Geophysical Review Letters*, 24, 257–260

Deser, C., & Blackmon, M.L. (1995). On the Relationship between Tropical and North Pacific Sea Surface Temperature Variations. *Journal of Climate*, 8, 1677–1680

Deser, C.M., Alexander, A., & Timlin, M.S. (1996). Upper-Ocean Thermal Variations in the North Pacific during 1970-1991. *Journal of Climate*, 9, 1840–1855

- Ebbesmeyer, C.C., Cayan, D.R., McLain, D.R., Nichols, F.H., Peterson, D.H., & Redmond, K.T. (1991). 1976 step in the Pacific climate: Forty environmental changes between 1968-75 and 1977-1984. *In Proc. 7th Ann. Pacific Climate Workshop, Calif. Dept. of Water Resources, Interagency Ecol. Stud. Prog. Report 26.*
- Frankignoul, C., & Hasselmann, K. (1977). Stochastic climate models. Part II: Application to sea-surface temperature anomalies and thermocline variability. *Tellus*, 29, 284–305
- Frey, H., Latif, M., & Stockdale, T. (1997). The Coupled GCM ECHO-2, Part I: The Tropical Pacific. *Monthly Weather Review*, 125, 703–720
- Ghil, M. (1997). The SSA-MTM Toolkit: applications to analysis and prediction of time series. *Proceedings of the SPIE - The International Society for Optical Engineering*, 3165, 216–230
- Goddard, L., & Graham, N.E. (1997). El Niño in the 1990s. *Journal of Geophysical Research*, 102, 10423–36
- Goodman, J., & Marshall, J. (1999). A model of decadal middle-latitude atmosphere-ocean coupled modes. *Journal of Climate*, 12, 621–641
- Graham, N.E., Barnett, T.P., Wilde, R., Ponater, M., & Schubert, S. (1994). On the roles of tropical and midlatitude SSTs in forcing interannual to interdecadal variability in the winter northern hemisphere circulation. *Journal of Climate*, 7, 1416–41
- Grotzner, A., Latif, M., & Timmermann, A. (1999). Interannual to Decadal Predictability in a Coupled Ocean-Atmosphere General Circulation Model. *Journal of Climate*, 12, 2607–2624
- Hasselmann, K. (1976). Stochastic climate models. I. Theory. *Tellus*, 28, 473–485
- Horel, J.D., & Wallace, J.M. (1981). Planetary-scale atmospheric phenomena associated with the Southern Oscillation. *Monthly Weather Review*, 109, 813–829
- Jin, F.F. (1997). A theory of interdecadal climate variability of the North Pacific ocean-atmosphere system. *Journal of Climate*, 10, 1821–1835
- Kiehl, J.T., Hack, J.J., Bonan, G.B., Boville, B.A., Briegleb, B.P., Williamson, D.L., & Rasch, P.J. (1996). Description of the NCAR Community Climate Model (CCM3). Technical Report "NCAR Technical Note TN-420", Available from National Center for Atmospheric Research, Boulder, CO.

Latif, M., & Barnett, T.P. (1994). Causes of Decadal Climate Variability over the North Pacific and North America. *Science*, 266, 634–637

Latif, M., & Barnett, T.P. (1996). Decadal Climate Variability over the North Pacific and North America: Dynamics and Predictability. *Journal of Climate*, 9, 2407–2423

Lau, N.C. (1997). Interactions between global SST anomalies and the midlatitude atmospheric circulation. *Bulletin of the American Meteorological Society*, 78, 21–33

Levitus, S. (1994). World ocean atlas 1994. Technical Report ””, Available from U.S. Dept. of Commerce, National Oceanic and Atmospheric Administration.

Mantua, N.J., Hare, S.R., Zhang, Y., Wallace, J.M., & Francis, R.C. (1997). A Pacific Interdecadal Climate Oscillation with Impacts on Salmon Production. *Bulletin of the American Meteorological Society*, 78, 1069–1079

Miller, A.J., & Schneider, N. (2000). Interdecadal climate regime dynamics in the North Pacific Ocean: Theories, observations, and ecosystem impacts. *Progress in Oceanography*

Miller, A.J., Cayan, D.R., Barnett, T.P., Graham, N.E., & Oberhuber, J.M. (1994). Interdecadal variability of the Pacific Ocean: model response to observed heat flux and wind stress anomalies. *Climate Dynamics*, 9, 287–302

Peng, S., Robinson, W.A., & Hoerling, M.P. (1997). The modeled atmospheric response to midlatitude SST anomalies and its dependence on background circulation states. *Journal of Climate*, 10, 971–987

Pierce, D.W., Barnett, T.P., Schneider, N., Saravanan, R., Dommenges, D., & Latif, M. (2000a). The role of ocean dynamics in producing decadal climate variability in the North Pacific. *Climate Dynamics (submitted)*

Pierce, D.W., Barnett, T.P., & Latif, M. (2000b). Connections between the Pacific Ocean tropics and midlatitudes on decadal time scales. *Journal of Climate*, 13, 1173–1194

Pierce, D.W., Kim, K-Y, & Barnett, T.P. (1996). Variability of the Thermohaline Circulation in an Ocean General Circulation Model Coupled to an Atmospheric Energy Balance Model. *Journal of Physical Oceanography*, 26, 725–738

Saravanan, R., & McWilliams, J.C. (1998). Advective ocean-atmosphere interactions: an analytical stochastic model with implications for decadal vari-

ability. *J. Clim.*, 11, 165–188

Trenberth, K.E., & Hurrell, J.W. (1994). Decadal atmosphere-ocean variations in the Pacific. *Climate Dynamics*, 9, 303–319

Venzke, S., Munnich, M., & Latif, M. (1999). On the Predictability of Decadal Changes in the North Pacific. *Climate Dynamics*, *in press*

Wallace, J.M., Smith, C., & Jiang, Q. (1990). Spatial Patterns of Atmosphere-Ocean Interaction in the Northern Winter. *Journal of Climate*, 3, 990–998

Weng, W.J., & Neelin, J.D. (1998). On the role of ocean-atmosphere interaction in midlatitude interdecadal variability. *Geophysical Review Letters*, 25, 167–170

White, W.B. (1995). Network design of a global observing system for gyre-scale upper ocean temperature variability. *Progress in Oceanography*, 36, 169–217

White, W.B., & Peterson, R. (1996). The Antarctic Circumpolar Wave in surface pressure, wind, temperature, and sea ice extent. *Nature*, 380, 699–702

Zhang, Y., Wallace, J.M., & Battisti, D.S. (1997). ENSO-like Interdecadal Variability: 1900-93. *Journal of Climate*, 10, 1004–1020

## Figure Captions

Figure 1. Expected spectrum for white noise forcing of an oceanic mixed layer. See text for symbol definitions.

Figure 2. Spectrum of the Pacific Decadal Oscillation (PDO), along with best fit AR(1) process (heavy line) and 95% confidence interval (dashed lines).

Figure 3. The PDO time series, and four AR(1) time series tuned to have the same lag-1 autocorrelation coefficient as the PDO. See text for identification of the PDO time series.

Figure 4. Multi-taper spectra of the time series of Fig. 3.

Figure 5. Leading EOF of latent heat flux ( $\text{W}/\text{m}^2$ ) from the ECHO2 coupled ocean-atmosphere model.

Figure 6. Left column: leading EOF of 500 hPa height anomaly, gpm. From top to bottom: for the case with the full-physics atmospheric model coupled to specified climatological SST conditions, a mixed-layer model with depths specified from observations, and a full physics ocean model, respectively. Right column: correlation map of the PC for the EOF in the corresponding left hand column with SST anomalies. (Note that there are no SST anomalies for the case with specified climatological SSTs.)

Figure 7. Regression ( $^{\circ}\text{C}/\text{standard deviation}$ ) between PC of the leading EOF of observed sea level pressure over the North Pacific and observed ocean temperatures as a function of depth during the period 1955-1994.

Figure 8. Ratio of the standard deviation of SSTs, for the ECHO2 full-physics coupled ocean-atmosphere divided by the ECHAM3/mixed layer ocean coupled model. Contour interval is 1.0.

Figure 9. Ratio of the spectral density of SST variability at the point 156 W, 40.5 N, for the ECHO2 full-physics coupled ocean-atmosphere divided by the ECHAM3/mixed layer ocean coupled model. Shaded area shows where the ratio is statistically significant.

Figure 10. Spectra of SST in the Kuroshio extension region for the ECHO2 coupled ocean-atmosphere model (top), for the stand-alone ocean model forced with saved monthly fluxes from the ECHO2 run (middle), and from the stand-alone ocean model forced with the same monthly fluxes randomly permuted in time (bottom). Dashed lines indicate the 95% confidence interval.

Figure 11. Observed temperature trend,  $^{\circ}\text{C}/\text{decade}$ , over the period 1945-1999.

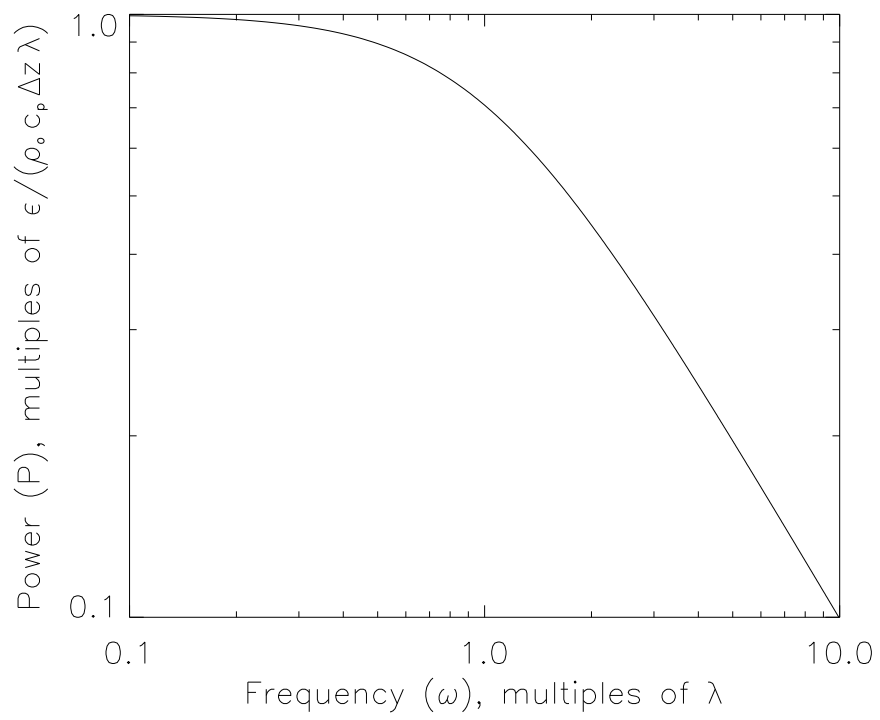


Fig. 1.

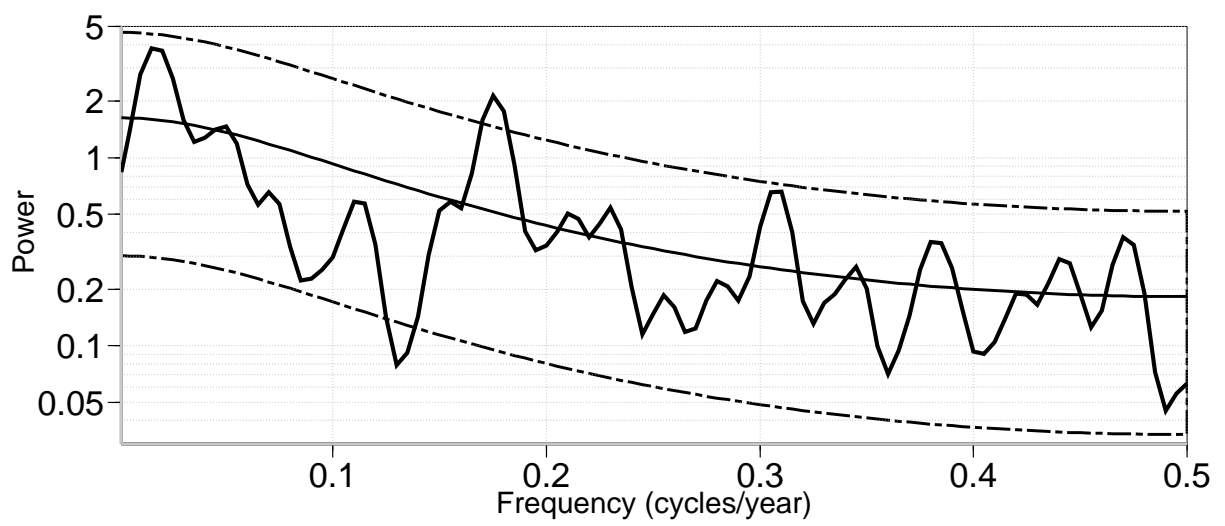


Fig. 2.



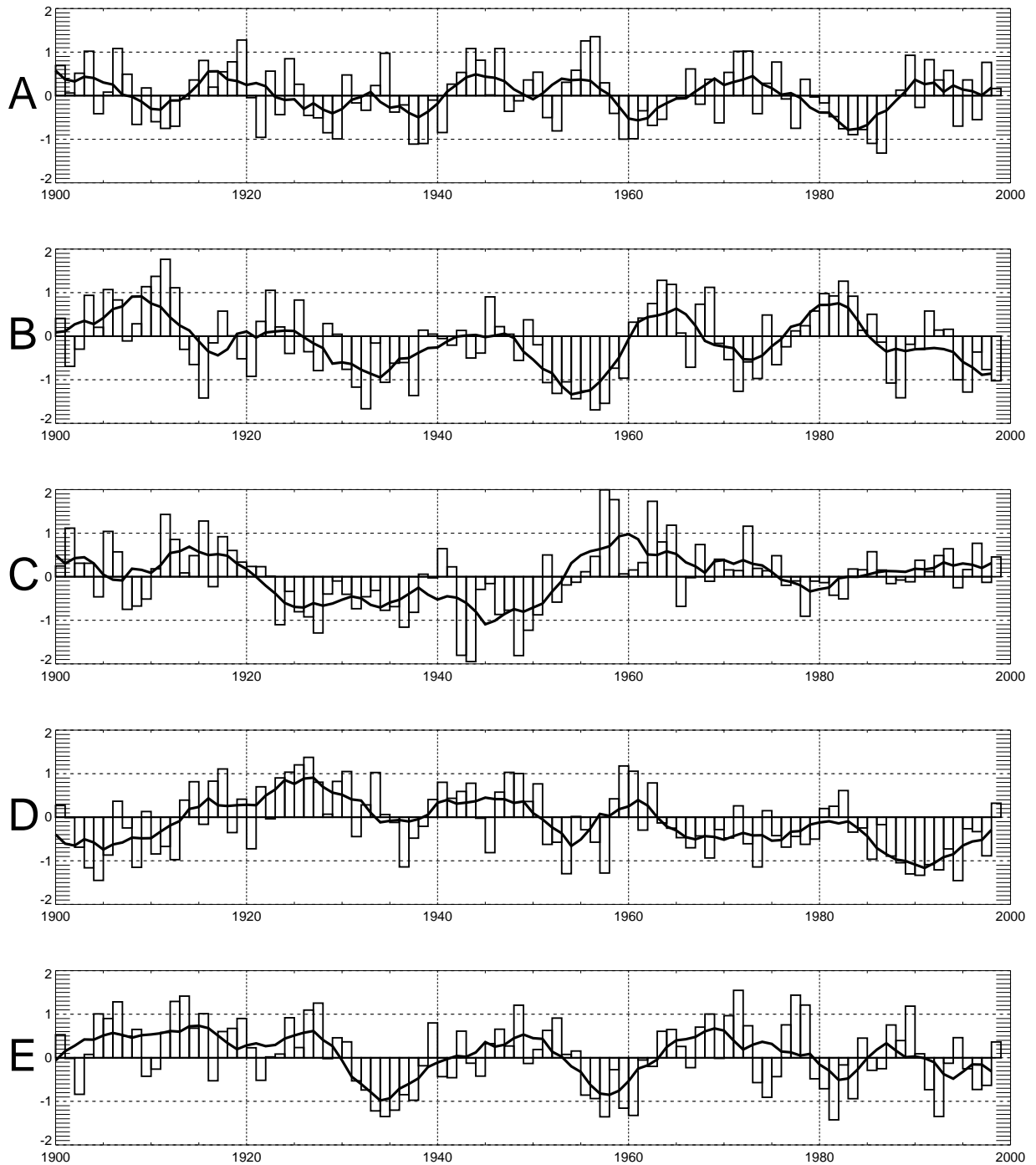


Fig. 3.

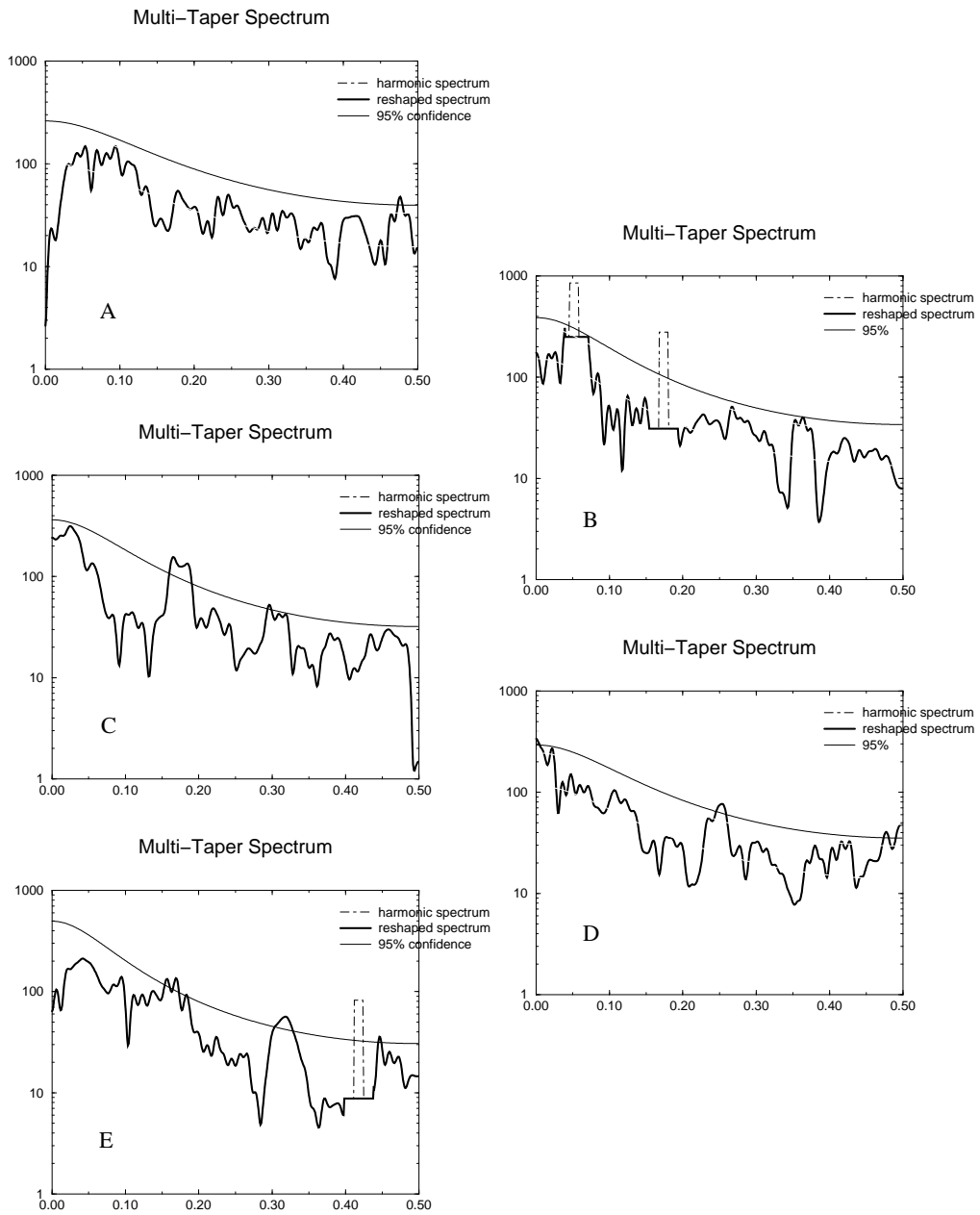


Fig. 4.

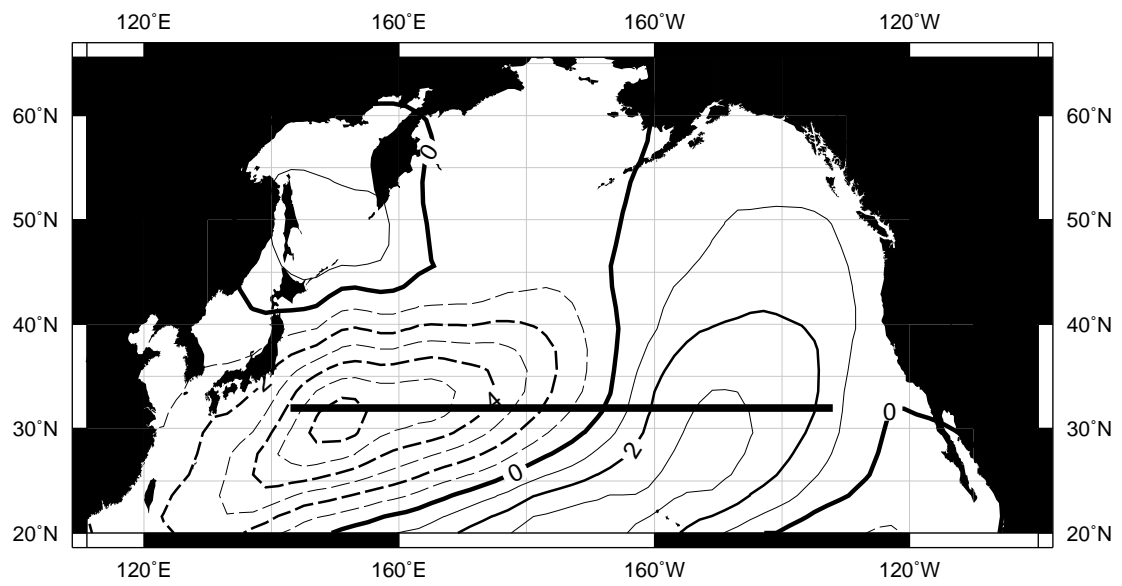


Fig. 5.

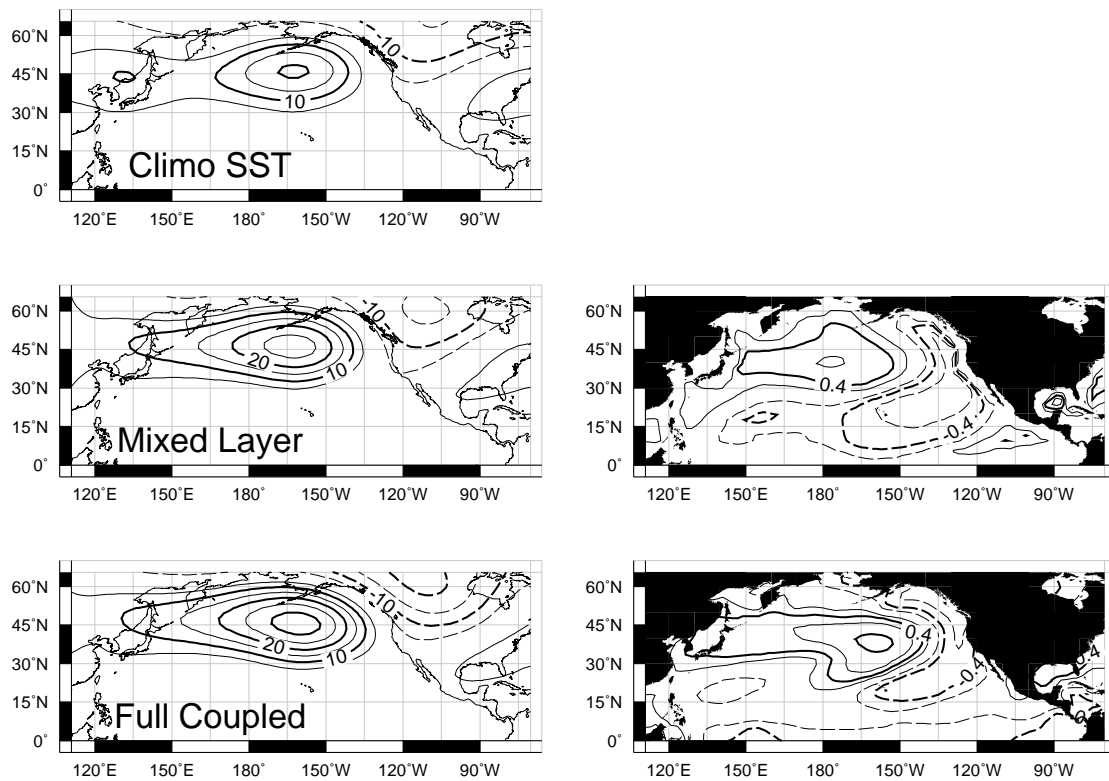


Fig. 6.

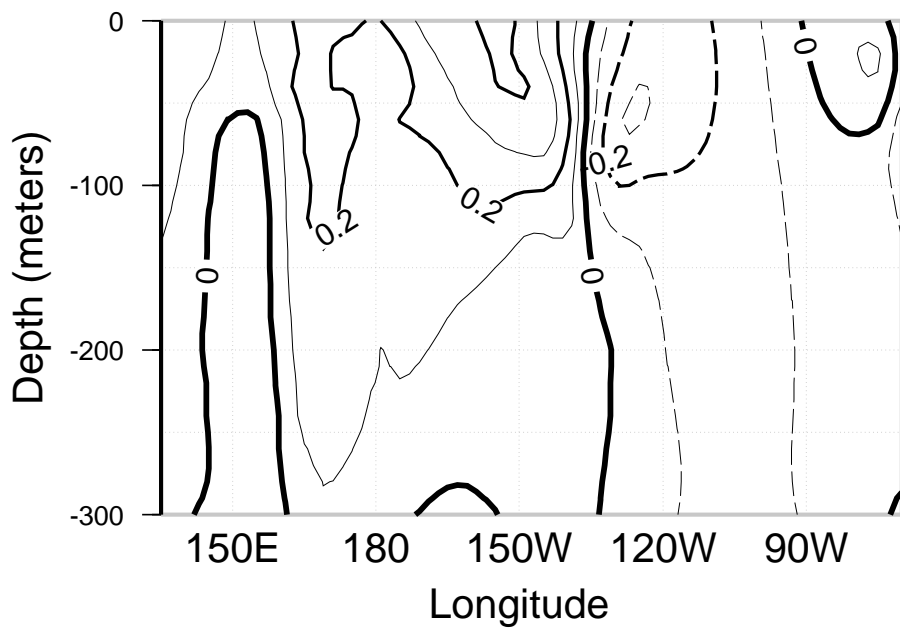


Fig. 7.

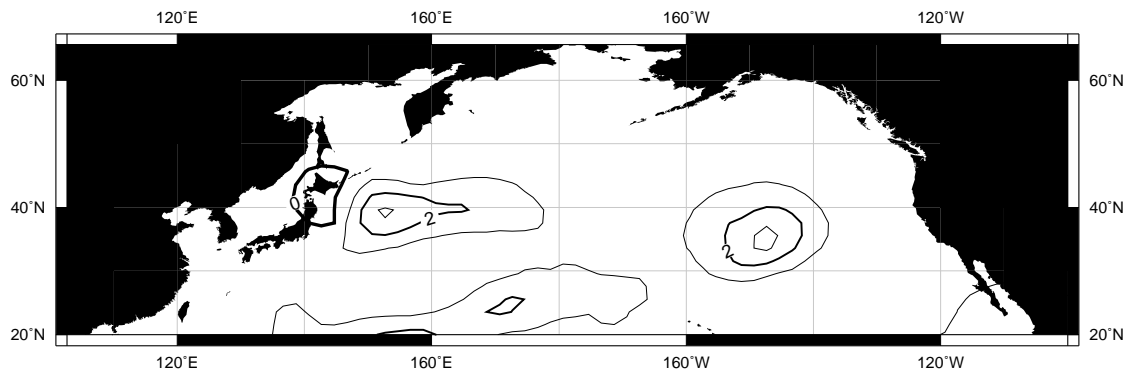


Fig. 8.

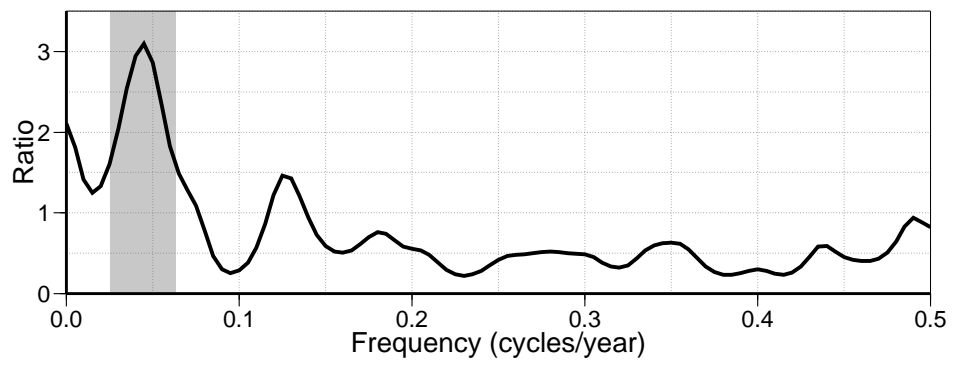


Fig. 9.

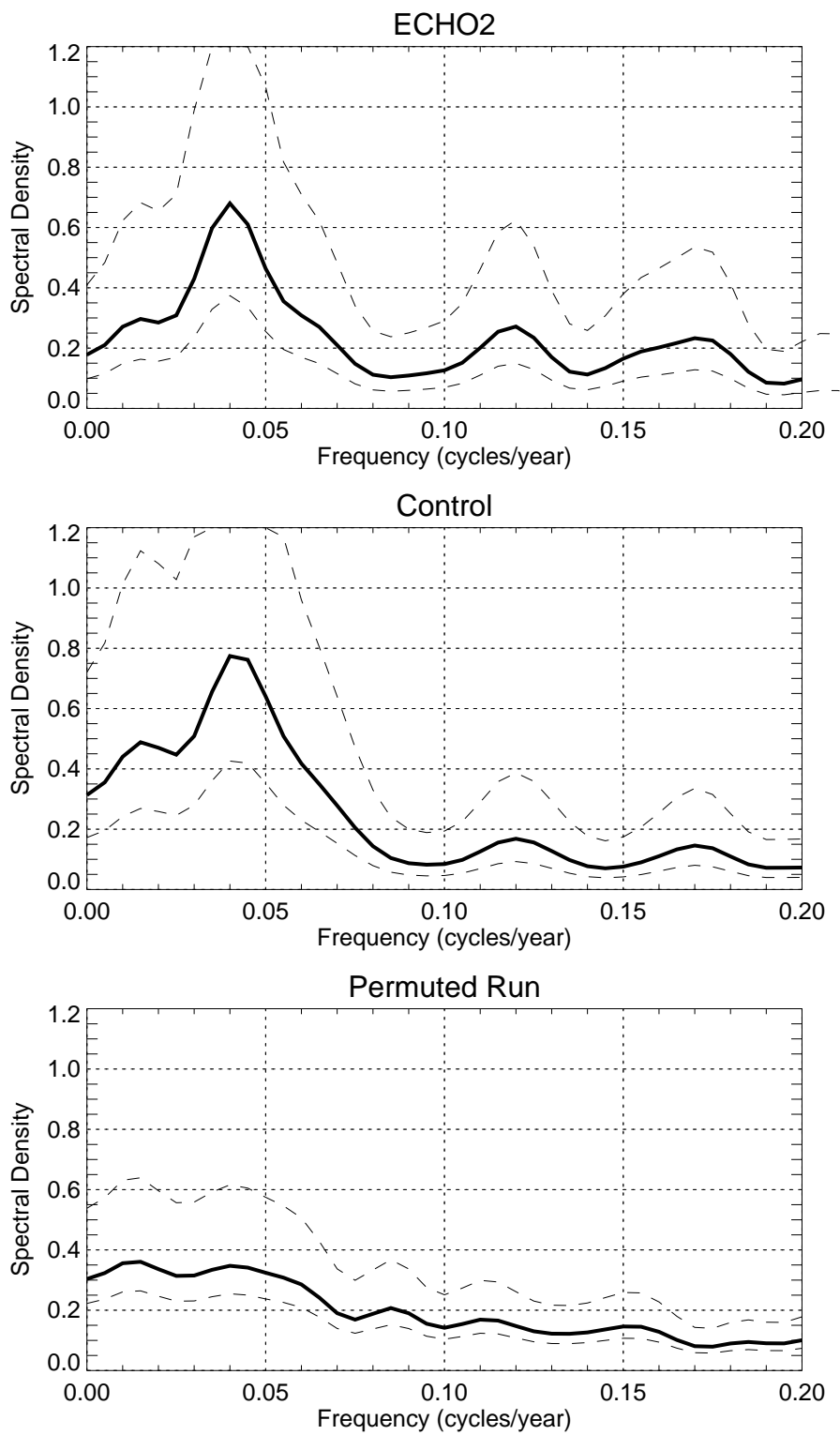


Fig. 10.



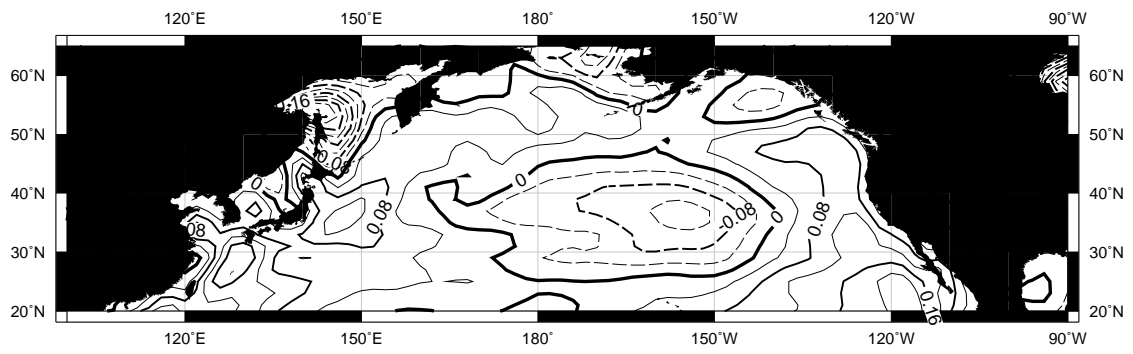


Fig. 11.